

# Small-Scale Variations of HI Spectra from Interstellar Scintillation

C.R. Gwinn

Physics Department, University of California, Santa Barbara, California, 93106

`cgwinn@condor.physics.ucsb.edu`

Received \_\_\_\_\_; accepted \_\_\_\_\_

arXiv:astro-ph/0105003v1 1 May 2001

## ABSTRACT

I suggest that radio-wave scattering by the interstellar plasma, in combination with subsonic gradients in the Doppler velocity of interstellar HI, is responsible for the observed small-scale variation in HI absorption spectra of pulsars. Velocity gradients on the order of 0.05 to 0.3 km s<sup>-1</sup> across 1 AU can produce the observed variations. I suggest observational tests to distinguish between this model and the traditional picture of small-scale opacity variations from AU-scale cloudlets.

*Subject headings:* ISM: clouds – ISM: structure – turbulence

## 1. INTRODUCTION

The small-scale structure of cold atomic hydrogen (HI) is an outstanding problem in the structure of the interstellar medium. Absorption spectra of the  $\lambda = 21$  cm hyperfine transition of the ground state show significant spectra changes over very small angles. Among the most extreme of these changes are observed for pulsars (Deshpande et al. 1992; Clifton et al. 1988; Frail et al. 1994). Absorption with inferred optical depth of  $\tau = 0.1$  to 2 in this line show apparent changes of  $\Delta\tau = 0.01$  to 0.1 over periods of a few months. Over this period, the motion of the pulsar typically carries the line of sight across tens of mas, or across several AU, for absorbing material at a distance of a few hundred pc. The most straightforward conclusion is that the HI consists largely of cloudlets with transverse dimensions of several AU, and optical depths of 0.01 to 0.1. This leads to surprisingly dense clouds which are far from pressure equilibrium with the rest of the interstellar medium (Heiles 1997). Small-scale structure of HI absorption has also been observed in spatially-varying absorption of extended continuum sources (Diamond et al. 1989; Davis, Diamond, & Goss 1996; Faison et al. 1998; Deshpande 1992; Dhawan, Goss, & Rodriguez

2000; Faison & Goss 2001). In this paper, I will consider changes in pulsar absorption quantitatively using a simple model, and discuss absorption by extended continuum sources only qualitatively.

I propose that the observed variations of pulsar absorption spectra arise from the interaction of interstellar scintillation with transverse gradients in Doppler velocity of HI. Interstellar scintillation is a well-understood phenomenon resulting from scattering by interstellar free electrons (Rickett 1977, and references therein). The observer receives scattered radiation from more than one path. Differences in radio-wave path length, from small-scale fluctuations in the density of interstellar free electrons, lead to random interference and so to scintillation. At the frequency of the HI line, absorption and refraction introduce additional changes in amplitude and phase of the interfering signals. If these additional changes differ among paths, line and continuum will scintillate differently. The additional differences among paths change rapidly with frequency, across the line; but only slowly with time.

I suggest that this differing HI absorption results from a gradient in Doppler velocity of the HI across the scattering disk. At a given observing frequency, absorption by HI at a range of Doppler velocities in the gradient will block a strip of radiation, eliminating some of the paths that would otherwise reach the observer and contribute to the interference pattern. The location of the strip changes with frequency, blocking different paths and changing the interference pattern in different ways. To either side of the blocked strip, resonant refraction will change the path length and change the phase along paths. The consequence is an interference pattern that changes sensitively with frequency across the absorption line. This pattern changes with time, at the timescale of scintillation.

In §2 of this paper, I present a simple mathematical model for the effects of a transverse gradient in the Doppler velocity of HI, or any variation in HI absorption, in combination

with interstellar scattering. In §3 I estimate the Doppler velocity gradient required to produce the observed small-scale variations of HI spectra, and compare these gradients with those inferred by other observations and those expected in the absorbing-cloudlet model. In §4 I summarize the results.

## 2. MODEL

### 2.1. Scattering by Free Electrons

In this section I present a specific model for variations in the HI line, from sub-AU structure of HI clouds. Consider a pulsar at distance  $d$  from the Earth, scattered by intervening interstellar plasma. In general scattering material will be distributed along the line of sight; however, a single screen of phase-changing material at  $d/2$  conveniently represents effects of scattering. The electric field at the observer can be represented as a Kirchoff integral over the screen (Gwinn et al. 1998). The observer sees changes in the intensity of the source because of fortuitous reinforcement or cancellation of radiation from different points on the scattering screen. We suppose that the scattering is strong: in this case, phase differences between paths are many radians. We also assume that the radiation can be treated in the Gaussian field approximation, in which the phase changes introduced at different points on the screen are taken to be completely uncorrelated, so that the summation of electric field from different paths at the observer has the character of a random walk. However, the argument here can be generalized to weak or refractive scattering, and to power-law or other spectra for the phase variations over the screen. In this paper I consider strong diffractive scattering, for greatest physical insight.

We approximate the Kirchoff integral for electric field at the observer as a phasor sum:

$$E = \sum_{\iota} \frac{e^{i\phi_{\iota}}}{H_{\iota}}. \quad (1)$$

The phase  $\phi_i$  is the sum of that introduced by the scattering screen,  $\Phi(\mathbf{x}_i)$ , and a geometric phase from path length for the stationary phase point at  $\mathbf{x}_i$ :  $\phi_i = \Phi(\mathbf{x}_i) + kx_i^2(4/d)$ . At a stationary phase point, the gradient of screen phase cancels the gradient of geometric phase. In the stationary phase approximation only stationary phase points contribute to the Kirchoff integral. The wavenumber is  $k = 2\pi/\lambda$ . The weight of each phasor,  $1/H_i$ , corresponds to an area on the screen. The distribution of stationary phase points, weighted by  $1/H_i$ , is approximately a Gaussian distribution, with full width at half maximum  $\theta_H d/2$ , in the Gaussian-field approximation. The size of the region from which the observer receives radiation acts analogously to a lens, to produce a diffraction pattern with lateral scale  $S_{ISS} \approx \sqrt{4 \ln 2} \lambda / \theta_H$  in the plane of the observer.

The intensity at the observer is the square modulus of electric field,

$$I_c = EE^* = \sum_{i,j} \frac{e^{i(\phi_i - \phi_j)}}{H_i H_j}. \quad (2)$$

Here the subscript “c” indicates that the intensity is in the continuum, to distinguish it from line radiation. The intensity varies with time, with typical timescale  $t_{ISS} = S_{ISS}/V_\perp$ , as the proper motions of pulsar and screen carry the line of sight through the scattering material at speed  $V_\perp$ . The intensity also varies with observing frequency  $\nu$ , with typical frequency scale, or “decorrelation bandwidth,”  $\Delta\nu \approx (8 \ln 2 / 2\pi)c / (d\theta_H^2)$ , because radiation paths that produce cancellation at one observing wavelength may reinforce at another. Lambert & Rickett (1999) give precise expressions for these relations for cases of power-law spectra of density fluctuations. In strong scattering, decorrelation bandwidth is much smaller than the observing frequency. In weak scattering the bandwidth of scintillations is of order the observing frequency. Because the electron-density fluctuations responsible for scattering are dispersive, most pulsars are weakly scattered at sufficiently high frequencies, and strongly scattered at low frequencies.

Table 1 presents the scintillation bandwidths for pulsars with observed small-scale

structure in the HI line. For nearly all objects, the decorrelation bandwidth of scintillations is somewhat less than the observing frequency, indicating strong scattering. However, the decorrelation bandwidth is much greater than width of the HI line, of  $\approx 3$  to  $20 \text{ km s}^{-1}$ , or  $\approx 0.03$  to  $0.1 \text{ MHz}$ , and indeed is much greater than the spectral range typically observed for absorption studies. The exceptions are pulsars B0540+23 and B1557–50. For B0540+23 the decorrelation bandwidth of  $0.2$  to  $0.5 \text{ MHz}$  is larger than the linewidth, but not larger than the width of a typical spectrum; Frail et al. (1994) describe how they remove the variable baseline introduced by scintillation for this object. For B1557–50 the reported decorrelation bandwidth is much less than the linewidth. We will consider this object separately.

## 2.2. Effects of HI

At the frequency of the  $\lambda = 21 \text{ cm}$  line, intervening HI will introduce both absorption and optical path length. The optical depth  $\tau_{HI}$  and the phase change  $\phi_{HI}$  parametrize these effects. Both are proportional to the column density of HI. The Kramers-Kronig relations relate  $\tau_{HI}$  and  $\phi_{HI}$  to one another via integrals over all frequencies. Here we note that, as a rule of thumb,  $\phi_{HI}$  at the line edge, in radians, is on the order of  $\frac{1}{2}\tau_{HI}$  at line center. The factor of  $\frac{1}{2}$  arises from the fact that  $\tau$  is the logarithmic decrease of intensity, rather than electric field.

Suppose that the HI consists of a background distribution, uniform over the screen, and a small fraction that has varying properties over the screen. Within the absorption line, the background distribution will introduce a fractional change in amplitude and a phase rotation, both uniform for all phasors. The varying part will change each phasor differently and change the phasor sum  $E$ . Figure 1 shows the geometry schematically, for the particular case where variation in absorption arises from a gradient of Doppler velocity.

A simple mathematical model describes the effects of absorbing HI in the language of § 2.1. Let the constant part have optical depth  $\tau_0$  and phase changes of  $\varphi_0$ , and the varying part have optical depth  $\delta\tau_i$  and phase change  $\delta\varphi_i$ , at location  $\mathbf{x}_i$  on the screen. We suppose that  $\delta\tau$  has zero mean, when averaged over the scattering disk, so that  $\delta\tau_i$  takes on positive and negative values. The electric field at the observer, at a frequency within the HI line, is then a generalization of Eq. 1:

$$E_{HI} = e^{-\frac{1}{2}\tau_0 + i\varphi_0} \sum_i \frac{e^{i\phi_i}}{H_i} e^{-\frac{1}{2}\delta\tau_i + i\delta\varphi_i}. \quad (3)$$

Through first order in  $\delta\tau$  and  $\delta\varphi$ , the intensity on the line is:

$$I_{HI} = |E_{HI}|^2 \approx e^{-\tau_0} \left\{ \left| \sum_i \frac{e^{i\phi_i}}{H_i} \right|^2 + \text{Re} \left[ \sum_i \frac{e^{i\phi_i}}{H_i} (\delta\tau_i + i2\delta\varphi_i) \sum_j \frac{e^{-i\phi_j}}{H_j} \right] \right\}. \quad (4)$$

Studies of the distribution of HI measure the normalized spectrum. The normalized absorption of the line is:

$$\frac{I_c - I_{HI}}{I_c} \approx 1 - e^{-\tau_0} - e^{-\tau_0} \text{Re} \left[ \frac{\sum_i \frac{e^{i\phi_i}}{H_i} (\delta\tau_i + i2\delta\varphi_i)}{\sum_i \frac{e^{i\phi_i}}{H_i}} \right]. \quad (5)$$

The first two terms on the right-hand side give the optical depth of the constant part of the distribution of HI, as expected. The last term describes the different scintillation on the line and away from the line, because of the effects of the additional optical depth and phase of the randomly-varying part of the HI distribution.

The depth of the normalized absorption spectrum,  $(I_c - I_{HI})/I_c$ , thus includes a randomly-varying term. This term is the quotient of 2 random factors. The variance of the denominator is the mean intensity of the continuum:  $\langle |\sum_i e^{i\phi_i}/H_i|^2 \rangle = \langle I_c \rangle$ . Under the assumption that the small-scale fluctuations in electron density responsible for scattering are uncorrelated with the varying part of the HI distribution, the dispersion of the numerator is  $(\langle |\delta\tau|^2 \rangle + 4\langle |\delta\varphi|^2 \rangle) \langle I_c \rangle$ .

I assume that the sums in the numerator and denominator have the statistics of uncorrelated random walks. This is the case if the Gaussian field approximation holds, as is the case in strong scattering on short timescales. (The statistics of HI absorption and refraction are relatively unimportant, as long as electron-density fluctuations are highly uncorrelated). For weaker scattering, correlations between numerator and denominator can appear: for example, electron-density fluctuations  $\phi$  and optical depth can both change linearly with position. One might expect the variations of the quotient to be even greater in this case.

The appendix presents the distribution of the quotient of uncorrelated random walks. The mean square and higher moments of this distribution do not converge. However, a “typical” value of the quotient is the quotient of the standard deviations of the distributions, or  $\sqrt{\langle|\delta\tau|^2 + 4\langle|\delta\varphi|^2\rangle}$  in our case. Because  $\delta\tau$  and  $2\delta\varphi$  reach comparable maximum values (although at different frequencies), we expect that the quotient will have magnitude  $\sigma_{\delta\tau} = \langle|\delta\tau|^2\rangle$ .

We thus expect variations in intensity across the line with typical amplitude  $\Delta I/I_c \approx e^{-\tau_0} \sigma_{\delta\tau}$ . This variation will change amplitude on the timescale for scintillation,  $t_{ISS}$ . On this timescale the sums in the numerator and denominator of Eq. 5 will change. Of course, the intensity of the continuum  $I_c$  will change on the same timescale; however, these intensity variations have bandwidth much broader than the observed spectrum, and will be removed by averaging in time, for most pulsars with observed variation of HI spectra.

### 2.3. Velocity Gradients of HI

I suggest that the variations in opacity  $\delta\tau$  arise from velocity gradients. A cloud with opacity  $\tau_c$  and velocity different  $\Delta V$  across length  $L$  will show an opacity variation



of  $(\Delta V/C)\tau_c$  across that length, at observing frequencies near the rest frequencies of the cloud. Here  $C$  is the thermal velocity in the cloud,  $C = \sqrt{k_B T/\mu}$ , where  $T$  is the kinetic temperature,  $\mu$  is the mean molecular weight, and  $k_B$  is Boltzmann’s constant. We take the opacity difference as  $\sigma_{\delta\tau} = (\Delta V/C)\tau_c$  and the length  $L$  as the linear size of the scattering disk:  $L = \theta_H d/2$ .

The scintillation will differ at the frequency of the absorption line and in the continuum. Both will scintillate, but not in perfect proportion. Indeed, because  $\delta\tau$  and  $\delta\varphi$  vary with frequency, different parts of the line will scintillate differently. Figure 2 shows a simulation of scintillation over a frequency range that includes a line with a Gaussian absorption profile, and associated phase change, using a phasor sum (Gwinn et al. 1998).

### 3. COMPARISON AND DISCUSSION

#### 3.1. Comparison with Observations

Table 2 lists pulsars with observed variations in HI absorption. The table gives the largest  $\Delta I/I_c$  observed at each epoch. Typical observed variations in intensity are  $\Delta I/I_c \approx 0.03$ , and the depths of the normalized absorption spectra are typically  $(I_c - I_{HI})/I_c \approx 0.7$ . For scintillation to explain this typical case thus requires  $\sigma_{\delta\tau} \approx 0.03/0.7 \approx 0.04$ . If all absorption along the line of sight participates in forming these gradients, this requires velocity differences of  $\Delta V \approx 0.04C$  across the diameter of the scattering disk,  $L = \theta_H d/2$ . This calculation yields the values displayed in Table 3.

Among the objects in Table 2, two show particularly large  $\Delta I/I_c$ . These 2 events were the first reported, and first drew attention to the phenomenon. Pulsar B1557 – 50 shows  $\Delta I/I_c = 0.5$  (Deshpande et al. 1992). However, this pulsar is by far the most strongly scattered in the sample, with estimated angular broadening of 121 mas. The scattering disk

diameter is thus 300 AU. In principle, a weak gradient of  $0.003 \text{ km s}^{-1}$  can produce the result. However, the scintillation bandwidth is estimated as 160 Hz, and the scintillation timescale is probably only a few seconds. Thus, a single observation averages over many scintillations, and the scintillation model discussed here is unlikely to contribute in this particular case. This object represents an important exception to the relatively similar scattering properties of the other pulsars in the sample.

Pulsar B1821 + 05 shows  $\Delta I/I_c = 0.52$ . The change in the line was very narrow in frequency, with a Doppler width of  $< 1.2 \text{ km s}^{-1}$ , much smaller than the absorption linewidth of  $25 \text{ km s}^{-1}$ . I suggest that this is an unusual event, perhaps one of the extreme excursions responsible for the nonconvergence of the mean square of the distribution of the quotient.

Table 3 shows the gradients in Doppler velocity required across 1 AU, for each of the pulsars with observed variability of HI absorption. For most pulsars I give a range of estimated gradients. This range includes both the variety of  $\Delta I/I_c$  reported, and the differences among measurements of the decorrelation bandwidth. Because greatest  $\Delta I$  across the line is recorded at each epoch, and because the mean square and higher moments of the expected distribution do not converge, theseXS inferred gradients are more likely to be overestimates than underestimates. Lack of accurate measurements of angular broadening also contributes to the breadth of the range. Table 3 estimates angular broadening from decorrelation bandwidth as  $\theta_H = \sqrt{16\pi \ln 2 c/\Delta\nu d}$ . This estimate is likely to be rather poor for nearby objects such as those in the table (Britton, Gwinn, & Ojeda 1998), although it is accurate to within about a factor of 2 for more strongly-scattered objects (Gwinn, Bartel, & Cordes 1993). In summary, interstellar scattering and gradients in Doppler velocity of about  $0.05$  to  $0.3 \text{ km s}^{-1} \text{ AU}^{-1}$  can produce the observed variations in HI absorption.

### 3.2. Observed Gradients in Doppler Velocity

Although the lengths  $L = \theta_H d$  are quite small, by the standard of typically observed lengths in the interstellar medium, the inferred velocity differences  $\Delta V$  are small as well. Interstellar clouds invariably support turbulent velocities of several times thermal velocity. The widths of interstellar lines are consequently greater than those resulting from temperature of the gas by a factor of 2 to 3, tracing this turbulence (Mebold et al. 1982). In particular, the 21-cm absorption lines of pulsars observed for studies of small-scale structure commonly have widths of 2 to 3 km s<sup>-1</sup>, whereas the 50 to 100 K temperature of the gas would result in Doppler widths of 0.5 to 1 km s<sup>-1</sup>. These broader linewidths persist at even the highest angular resolutions observed.

Studies of the distribution of HI absorption against extended continuum sources may also be affected by scintillation, as discussed in § 3.6 below. Nevertheless, it is interesting to compare velocity gradients inferred from such studies with those required to produce small-scale structure of HI absorption for pulsars. As an example, Faison et al. (1998) observe a gradient of about 2.5 km s<sup>-1</sup> across about 30 mas, toward the source 3C138. For an absorber distance of 200 pc and a thermal velocity of 1 km s<sup>-1</sup>, this corresponds to a gradient of 0.4  $C/AU$ , comparable to the largest of those inferred from the scintillation model, as shown in Table 3.

### 3.3. Comparison with Cloudlet Model

Comparison velocity variations in the scattering model proposed here with density variations required in the cloudlet picture is illuminating. Under the assumption of rough balance between ram pressure and thermal pressure, a velocity difference  $\Delta V$  corresponds to a density difference  $\Delta \rho \approx \rho V \Delta V / C^2$ , where  $\rho$  is the density and  $V$  is a typical random

fluid velocity. The typical random velocity inferred from linewidth is about the thermal velocity, so  $\Delta\rho \approx \rho\Delta V/C$ . Thus, in the scintillation model, the velocity differences of about 0.05 to 0.3  $C$  correspond roughly to density differences of 5% to 30% across 1 AU.

In the traditional cloudlet model, with spherical cloudlets, the required density differences are of order a factor of 300 (Heiles 1997). The discrepancy is ameliorated if HI lies in sheets or filaments; it is aggravated by the necessity that  $H_2$  accompany the HI. These density differences are expressed across about 30 AU, the size of the clouds. In the absence of some additional confining mechanism, these clouds will evolve over the sound crossing time, or about 150 yr. It would be surprising if that evolution did not result in gradients of the sound speed across 1 AU, ample to produce variations in intensity by the scattering mechanism proposed here. Thus, even if discrete, dense cloudlets exist, the scattering mechanism proposed here should still play a role.

### 3.4. Observational Test

Small-scale structure of HI absorption due to scintillation will vary more rapidly than structure due to absorbing cloudlets. Intensity variations from scintillation vary on the scintillation timescale  $t_{ISS} = \sqrt{4 \ln 2} \lambda / (\theta_H V_\perp)$ . The timescale for variations from absorbing, intervening cloudlets can be no shorter than the time required for the scattering disk to move by its own width,  $t_r = \theta_H (d/2) / V_\perp$ , sometimes called the “refractive timescale”. In strong scattering,  $t_r$  is much longer than  $t_{ISS}$ . Indeed,  $t_{ISS}/t_r \approx \Delta\nu/\nu$ . With  $\Delta\nu/\nu \approx 0.2$  to 0.01, as shown in Table 1 most pulsars studied for small-scale variations of HI absorption are in strong scattering. Exceptions are pulsars B0950+08, which is in weak scattering and shows no absorption, and B1557–57, which is far into strong scattering, as discussed above. For the other pulsars, observations of changes in absorption spectra on timescales  $t_{ISS}$  would greatly strengthen the argument that scintillation, rather than absorbing cloudlets,

is responsible for small-scale structure of the HI absorption line.

A measurement of the average intensity of a scintillating source must be averaged over about 50 scintillations to produce a reproducible result, largely because a few strong scintillations dominate sums (Gwinn, Bartel, & Cordes 1993). Measurements converge even more slowly near the transition between weak and strong scattering, because the fractional modulation is great, up to  $\Delta I/I \approx \sqrt{3}$ . Because most pulsars in the sample have scintillation timescales of a few thousand seconds, even observations of several hours can fail to eliminate effects of scintillation by time averaging.

Pulsar 0540+23 is an exception. It has a scintillation timescale short enough that spectra from several contiguous scintillation timescales could be observed and compared, and much shorter than the refractive timescale. Thus the timescale of variations of HI absorption for this object presents an important test of the origin of variations in HI absorption.

### 3.5. Structure on a Range of Scales

Deshpande (2000) points out that absorbing HI is likely to be distributed on a variety of length scales. As an extreme case, a large-scale gradient of optical depth will produce spectral variations over any scale large enough not to be smeared by scattering. In this case, the smallest scale showing spectral variations has nothing to do with the size of the cloud. A medium with structure on a variety of scales is most accurately described by a structure function, or equivalently, spatial spectrum.

If velocity gradients in HI combine with interstellar scintillation to produce small-scale structure of the HI absorption line, the structure function of that structure will reflect different physics at large and small scales. Effects of scintillation at the short length scale

$V_{\perp} t_{ISS} \ll 1$  AU and do not increase with further increases in length scale. Absorption by discrete clouds will become increasingly important with increasing scale, as effects of larger clouds become more important. Determination of the structure function, and the point at which the underlying physics changes, will help to understand interstellar HI as well as the origin of small-scale changes in absorption spectra.

### 3.6. Extended Continuum Sources and Weak Scattering

As noted above, small-scale variations of HI absorption have been observed toward several continuum sources (Diamond et al. 1989; Davis, Diamond, & Goss 1996; Faison et al. 1998; Dhawan, Goss, & Rodriguez 2000; Faison & Goss 2001). Such sources do not scintillate, because they are large enough to quench scintillation. More precisely, the source is large enough that different parts scintillate independently and cancel out.

I suggest scintillation could nevertheless explain the observed variations. Many of the sources may be in weak scintillation, where the maximum source size for scintillation is relatively large, and scintillation is quenched only slowly as source size increases. Moreover, the size relevant as a constraint, for resolved sources in weak scattering, is the resolution of the instrument rather than the size of the source. Analogously, stars twinkle, but planets do not; but a single point on a planet’s surface does twinkle. Thus, a single point on an extended radio source will show variations in HI absorption, if scattering by electron-density fluctuations and a gradient of Doppler velocity of HI are present.

Refractive scattering can also produce variations in surface brightness of extended sources (Narayan & Goodman 1989; Goodman & Narayan 1989; Mutel & Lestrade 1990). This refractive “mottling” of the source is not quenched by finite source size. Velocity gradients will not affect refractive scattering, unless they are very large; however,

higher-order polynomial variations can affect it. Although the extension of the formalism of this paper to extended sources is straightforward in principle, description of weak and refractive scintillation requires a more complicated formalism, and I defer it to a subsequent paper.

#### 4. SUMMARY

I have presented a simple model for the effects of absorption by HI with a spatially-varying opacity  $\delta\tau$  on a scintillating pulsar. The scintillation state is different on and off the line: both scintillate, but not synchronously. The bandwidth of scintillation of the continuum is set by the phase differences among different paths, and is much broader than the line; the bandwidth of scintillation on the line is set by variations in opacity, and is typically of order the thermal linewidth.

Gradients in Doppler velocity of the absorbing HI can produce relative scintillations of line and continuum. Gradients of order 0.05 to 0.3 times the thermal velocity, across 1 AU produce effects comparable to the observed small-scale variations of HI absorption spectra. Such gradients are comparable to those inferred from observations. If discrete absorbing cloudlets produced the variation, they would result in comparable or larger gradients. The timescale of scintillation, on and off the line, is equal to the scintillation timescale, and can be much shorter than the minimum time for variations in intensity from absorbing cloudlets. This difference in timescales, and difference in structure functions, present possible observational tests of the scintillation model presented here.

I thank A. Deshpande and J. Heyl for useful discussions, and J. Weisberg for a copy of his thesis. The U.S. National Science Foundation provided financial support.

## A. QUOTIENT OF ELEMENTS DRAWN FROM UNCORRELATED GAUSSIAN DISTRIBUTIONS

Consider the distribution of  $f = u/x$ , where  $u$  and  $x$  are complex variables drawn from uncorrelated complex Gaussian distributions:

$$\begin{aligned} P(x) &= \frac{1}{2\pi\sigma_x^2} e^{-\frac{1}{2}|x|^2/\sigma_x^2} \\ P(u) &= \frac{1}{2\pi\sigma_u^2} e^{-\frac{1}{2}|u|^2/\sigma_u^2}. \end{aligned} \tag{A1}$$

In this case, the distribution of  $f$  is:

$$P(f) = \int du \int dx P(u)P(x) \delta(u/x - f), \tag{A2}$$

where  $\delta$  is the Dirac delta-function. I define

$$\begin{aligned} R_u &= \text{Re}[u], & I_u &= \text{Im}[u], \\ R_x &= \text{Re}[x], & I_x &= \text{Im}[x], \\ R_f &= \text{Re}[f], & I_f &= \text{Im}[f]. \end{aligned} \tag{A3}$$

Now one finds:

$$\begin{aligned} P(f) &= \frac{1}{4\pi^2\sigma_u^2\sigma_x^2} \int du \int dx e^{-\frac{1}{2}\frac{|u|^2}{\sigma_u^2}} e^{-\frac{1}{2}\frac{|x|^2}{\sigma_x^2}} \delta(\text{Re}[u/x] - R_f) \delta(\text{Im}[u/x] - I_f) \\ &= \frac{1}{4\pi^2\sigma_u^2\sigma_x^2} \int du \int dx e^{-\frac{1}{2}\frac{|x|^2}{\sigma_x^2}} e^{-\frac{1}{2}\frac{|u|^2}{\sigma_u^2}} \delta\left(\frac{R_u R_x - I_u I_x}{R_x^2 + I_x^2} - R_f\right) \delta\left(\frac{I_u R_x - R_u I_x}{R_x^2 + I_x^2} - I_f\right). \end{aligned} \tag{A4}$$

Note that:

$$|u|^2 = |f|^2 |x|^2 \tag{A5}$$

and

$$|x|^2 = R_x^2 + I_x^2. \tag{A6}$$



Using the rule  $\delta(x) = |a|\delta(ax)$ , one can then transform the  $\delta$ -functions, and the argument of the exponential in  $|u|^2$ , to find:

$$P(f) = \frac{1}{4\pi^2\sigma_u^2\sigma_x^2} \int du \int dx e^{-\frac{1}{2}\left(\frac{1}{\sigma_x^2} + \frac{|f|^2}{\sigma_u^2}\right)|x|^2} \frac{|x|^2}{I_x} \delta\left(I_u - \frac{R_f|x|^2}{I_x} + \frac{R_x R_u}{I_x}\right) I_x \delta(R_u - R_f R_x + I_f I_x), \quad (\text{A7})$$

where I have used the transformed first  $\delta$ -function to transform the second. The integrations over  $u$  and the complex phase of  $x$  are now trivial, and the distribution is:

$$P(f) = \frac{1}{2\pi\sigma_u^2\sigma_x^2} \int_0^\infty dX X^3 \exp\left\{-\frac{1}{2}\left(\frac{1}{\sigma_x^2} + \frac{|f|^2}{\sigma_u^2}\right)X^2\right\}, \quad (\text{A8})$$

where  $X = |x|$ . This can be evaluated to find

$$P(f) = \frac{\sigma_x^2\sigma_u^2}{\pi(\sigma_u^2 + |f|^2\sigma_x^2)^2}. \quad (\text{A9})$$

Note that the distribution function is normalized to unit volume over the complex plane, and that it is independent of the complex phase of  $f$ . This is a consequence of the fact that  $u$  and  $x$  are uncorrelated.

We can find the distribution of  $R_f = \text{Re}[f]$  by integrating  $P(f)$  over  $\text{Im}[f]$ . We find:

$$P(R_f) = \frac{\sigma_x\sigma_u^2}{2(\sigma_u^2 + R_f^2\sigma_x^2)^{3/2}}. \quad (\text{A10})$$

This distribution is normalized to unit area, over the real axis. It is symmetric about 0 and all odd moments of  $P(R_f)$  vanish. The mean of the absolute value of  $R_f$  is  $\langle |R_f| \rangle = 1$ . However,  $\langle R_f^2 \rangle$  and higher moments do not converge. Thus, one cannot speak of a mean squared value of  $R_f$ , and one cannot use this traditional measure to characterize the distribution. However, one can describe alternative measures. For example, a fraction  $P_0$  of the full distribution will lie between the values  $-f_0$  and  $+f_0$  when:

$$f_0 = \frac{\sigma_u P_0}{\sigma_x \sqrt{1 - P_0^2}}. \quad (\text{A11})$$

Thus, 50% of time the real part of the quotient  $R_f$  will lie at less than  $f_{50} = 1/\sqrt{3} \sigma_u/\sigma_x$ , 75% of the time  $R_f$  will lie at less than  $f_{75} = \sqrt{9/7} \sigma_u/\sigma_x \approx 1.1 \sigma_u/\sigma_x$ , and 95% of the time  $R_f$  will lie below  $f_{95} = \sqrt{391/39} \sigma_u/\sigma_x \approx 3 \sigma_u/\sigma_x$ .

## REFERENCES

- Bhat, N.D.R., Rao, A.P., & Gupta, Y. 1999, ApJS, 121, 483
- Britton, M.C., Gwinn, C.R., & Ojeda, M.J. 1998, ApJ, 501, L101
- Clifton, T.R., Frail, D.A., Kulkarni, S.R., & Weisberg, J.M. 1988, ApJ, 333, 332
- Cordes, J.M., Weisberg, J.M., & Boriakoff, V. 1985, ApJ, 288, 221
- Davis, R. J., Diamond, P. J., & Goss, W. M. 1996, MNRAS, 283, 1105
- Deshpande, A.A. 2000, MNRAS, 317, 199
- Deshpande, A.A., Dwarakanath, K.S., & Goss, W.M. 2000, ApJ, 543, 227
- Deshpande, A.A., McCulloch, P.M., Radhakrishnan, V., & Anantharamaiah, K.R. 1992, MNRAS, 258, 19P
- Dhawan, V., Goss, W.M., & Rodriguez, L.F. 2000, ApJ, 540, 863
- Diamond, P. J., Goss, W. M., Romney, J. D., Booth, R. S., Kalberla, P. M. W., & Mebold, U. 1989, ApJ, 347, 302
- Faison, M.D., Goss, W.M., Diamond, P.J., & Taylor, G.B. 1998, AJ, 116, 2916
- Faison, M.D., & Goss, W.M. 2001, AJ, in press
- Frail, D.A., Cordes, J.M., Hankins, T.H., & Weisberg, J.M. 1991, ApJ, 382, 168
- Frail, D.A., Weisberg, J.M., Cordes, J.M., & Mathers, C. 1994, ApJ, 436, 144
- Goodman, J., & Narayan, R. 1989, MNRAS, 238, 995
- Gupta, Y. 1995, ApJ, 451, 717

- Gwinn, C.R., Bartel, N., Cordes J.M. 1993, ApJ, 410, 673
- Gwinn, C.R., Britton, M.C., Reynolds, J.E., Jauncey, D.L., King, E.A., McCulloch, P.M.,  
Lovell, J.E.J., & Preston, R.A. 1998, ApJ, 505, 928
- Heiles, C. 1997, ApJ, 481, 193
- Lambert, H.C., & Rickett, B.J. 1999, ApJ, 517, 299
- Mebold, U., Winnberg, A., Kalberla, P.M.W., & Goss, W.M. 1982, A&A, 115, 223
- Mutel, R.L., & Lestrade, J.-F. 1990, ApJ, 349, L47
- Narayan, R. & Goodman, J. 1989, MNRAS, 238, 963
- Phillips, J.A., & Clegg, A.W. 1992, Nature, 360, 137
- Rickett, B.J., 1977, ARA&A, 15, 479

Table 1. Scattering Properties of Pulsars

Pulsar	Decorrelation	Scintillation	References
	Bandwidth <sup>a</sup>	Timescale <sup>b</sup>	
	$\Delta\nu$	$t_{ISS}$	
	(MHz)	(sec)	
B0540+23	0.2 to 0.5	58	1,2
B0823+26	160 to 180	550 to 940	2,3
B0950+08	weak	weak	4
B1133+16	280 to 900	390 to 800	2,3
B1557–50	0.00016		5
B1737+13	5 to 8		1
B1821+05	3.7 to 4.6	1500	1,2
B1929+10	770 to 648	1500 to 1900	2,3
B2016+28	30 to 130	4400 to 2500	2,3

<sup>a</sup>Scaled to frequency  $\nu = 1420$  MHz via  $\Delta\nu \propto \nu^{4.4}$ .

Ranges indicate range of observed values.

<sup>b</sup>Scaled to frequency  $\nu = 1420$  MHz via  $t_{ISS} \propto \nu^{1.2}$ .

Ranges indicate range of observed values.

References. — (1) Cordes, Weisberg & Boriakoff (1985); (2) Gupta (1995); (3) Bhat et al. (1999); (4) Phillips & Clegg (1992); (5) Rickett (1977).

Table 2. Reported Variations of HI Absorption

Pulsar	Epochs	Time Span (yr)	Normalized Absorption $(I_c - I_{HI})/I_c$	Fractional Intensity Change <sup>a</sup> $\Delta I_{HI}/I_c$	References
B0540+23	3	1.7	0.90	0.06, 0.08, 0.05	1
B0823+26	3	1.7	0.75	0.025, 0.045, 0.045	1
B0950+08	3	1.7	0	0	1
B1133+16	3	1.7	0.75	0.013, 0.043, 0.022	1
B1557–50	2	4	0.70	0.5	2
B1737+13	3	1.7	0.27	0.09, 0.06, 0.06	1
B1821+05	2	1	0.68	0.52	3,4
B1929+10	3	1.7	0.88	0.02, 0.009, 0.015	1
B2016+28	4	4.8	0.21	0.08, 0.03, 0.05	1

<sup>a</sup>Multiple entries reflect multiple epochs.

References. — (1) Frail et al. (1994); (2) Deshpande et al. (1992); (3) Clifton et al. (1988); (4) Frail et al. (1991).

Table 3. Inferred Velocity Gradient and Scale

Pulsar	Distance	Angular Broadening <sup>a</sup>	Length Scale	Velocity Gradient
	$d$	$\theta_H$	$L = \theta_H d / 2$	$\Delta V / (CL)$
	(kpc)	(mas)	(AU)	(km s <sup>-1</sup> AU <sup>-1</sup> )
B0540+23	3.54	3 to 5	5 to 9	0.015 to 0.04
B0823+26	0.38	0.5	0.3 to	0.15 to 0.3
B1133+16	0.27	0.2 to 0.4	0.12 to 0.2	0.10 to 0.6
B1557–50 <sup>b</sup>	6.30	121	303	0.003
B1737+13	4.77	0.6 to 0.8	1.3 to 1.7	0.04 to 0.08
B1821+05 <sup>c</sup>	3.0	1.0 to 1.2	1.8 to 2.0	0.4
B1929+10	0.17	0.3 to 0.4	0.14 to 0.15	0.14 to 0.3
B2016+28	1.10	0.3 to 0.7	0.3 to 0.7	0.05 to 0.3

<sup>a</sup>Estimated from decorrelation bandwidth and distance as  $\theta_H = \sqrt{16\pi \ln 2c / \Delta\nu d}$  (Gwinn, Bartel, & Cordes 1993).

<sup>b</sup>Long period between observations; variations may reflect changes in  $\tau_0$ .

<sup>c</sup>Large  $\Delta I / I_c$  is responsible for large gradient.

Note. — Parameter ranges indicate the observed ranges of  $\Delta\nu$  and  $\Delta I_{HI} / I_c$  in Table 1, and should be taken to represent the range in which the derived parameter is likely to lie, rather than an observational uncertainty, or the true range of variation of the parameter.

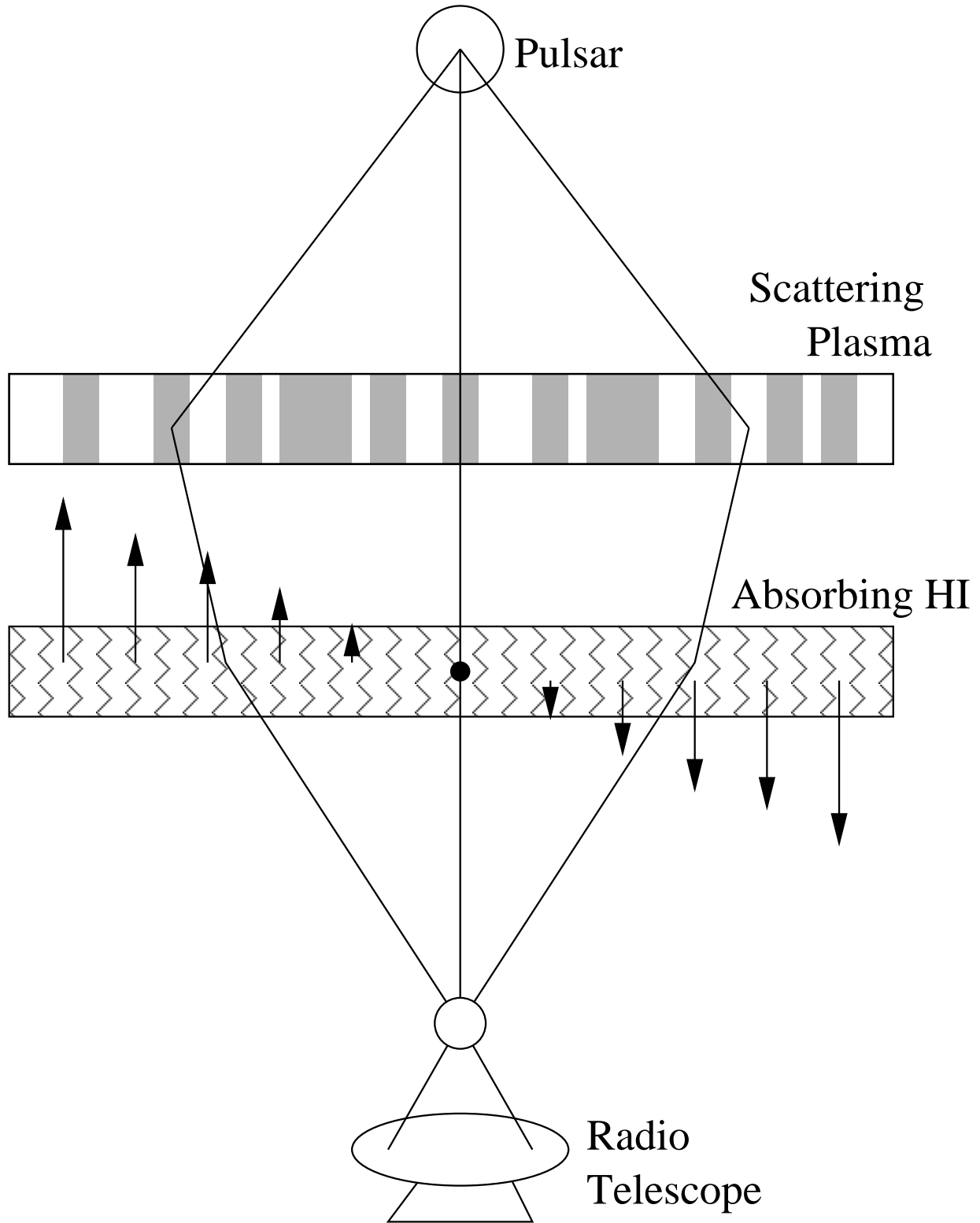


Fig. 1.— Schematic view of scattering of pulsar radiation by fluctuations in the free-electron density of the interstellar plasma, followed by absorption by HI with a transverse gradient of Doppler velocity.

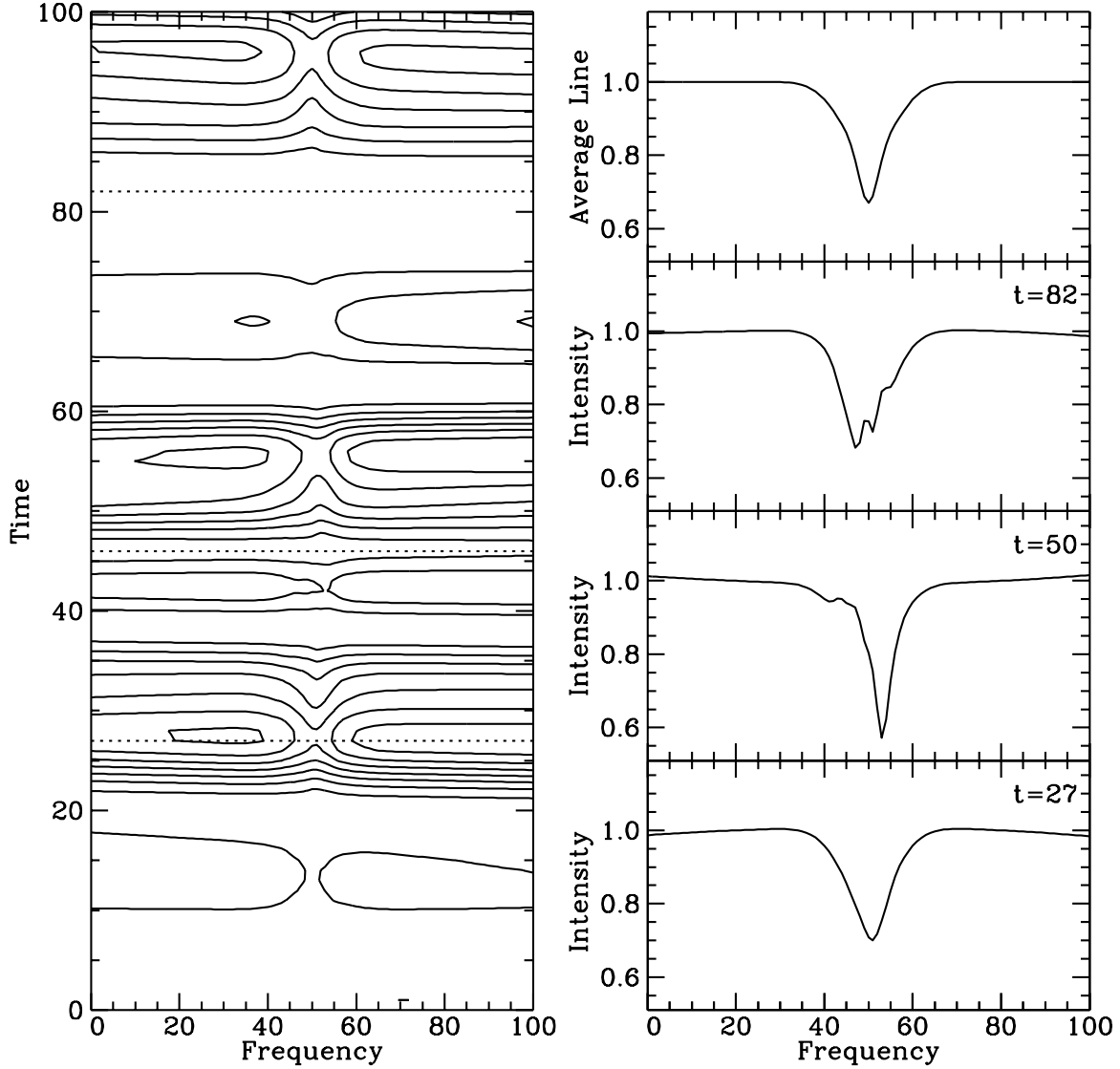


Fig. 2.— Simulation of small-scale variation in HI absorption via gradients in Doppler velocity. Left: Simulated dynamic spectrum, with HI line at center of band. Right: Upper panel shows average intensity spectrum. Lower panels show observed spectra at different times, as indicated by dotted lines on right plot. A slope has been removed from each spectrum. Model parameters are average opacity  $\tau_0 = 0.1$ , velocity gradients  $\Delta V = 0.8C$  across  $\theta_H d/2$  with opacity  $\sigma_{\delta\tau} = 0.1$ , and total linewidth of 3 times thermal linewidth.